Inorg. Chem. **2005**, *44*, 6930–6932

Structural Tuning of Ligand-Based Two-Electron Intervalence Charge Transfer

Julien Bachmann and Daniel G. Nocera*

Department of Chemistry, 6-335, Massachusetts Institute of Technology, 77 Massachusetts Avenue, Cambridge, Massachusetts 02139-4207

Received July 1, 2005

The lowest-energy optical transition of two-electron-oxidized porphyrinogens [$L^{\Delta}M$] is a ligand-based charge transfer. The color of the intermediary, two-electron mixed-valent oxidation state shifts from vermilion (λ_{max} = 480 nm) to yellow (λ_{max} = 270 nm) upon increasing the ionic radius of the central metal dication from Mg^{2+} to Zn^{2+} and Ca^{2+}. Structural, spectroscopic, and computational studies establish that the relative energies of the highest occupied and lowest unoccupied orbitals, between which the intervalence charge-transfer optical transition occurs, are modulated by the molecular dipole moment, which in turn depends on the only structural variable among the [$L^{\Delta}M$] compounds, the position of M^{2+} relative to the dianionic dipyrrole unit.

Intervalence charge transfer (IVCT) was defined within both theoretical[1−3] and experimental[4] frameworks soon after mixed valency was observed to give rise to an intense visible absorption in molecules[5] and solids.[6] In most cases, IVCT occurs between metals that differ by 1 in their formal oxidation state. The intensity and energy of IVCT in these systems depend on the electronic and metrical properties of the bridge linking the mixed-valent metal centers.[7−10] We have recently described an alternate form of mixed valency: one that is ligand-based and in which redox subunits differ in their formal oxidation states by 2.[11,12] Two-electron oxidation of the tetrapyrrole ring of zinc porphyrinogen is accompanied by spirocyclopropane ring formation upon C−C coupling between the α-carbons of neighboring pyrroles (Δ). The highest-energy occupied molecular orbitals (HOMOs) are localized on the reduced half of the macrocycle, whereas the lowest-energy unoccupied orbitals (LUMOs) are localized on the oxidized half of the porphyrinogen. A solvent-dependent visible transition characterizes the two-electron mixed-valent state of zinc porphyrinogen, [$L^{\Delta}Zn$],[11] arising from IVCT between the neighboring reduced and oxidized dipyrrole halves of the macrocycle. We now report the synthesis of [$L^{\Delta}M$] complexes with M = Mg and Ca. Together with the previously reported M = Zn system, this homologous series featuring spectroscopically silent central metal ions allows for a detailed investigation of the ligand-based IVCT transition of the $[L^{\Delta}]^{2-}$ macrocycle. Structural studies, augmented by density functional theory (DFT) computations, reveal that the IVCT energy of isostructural $[L^{\Delta}]^{2-}$ peripheries depends singularly on the position of the metal dication within the macrocycle.

Scheme 1

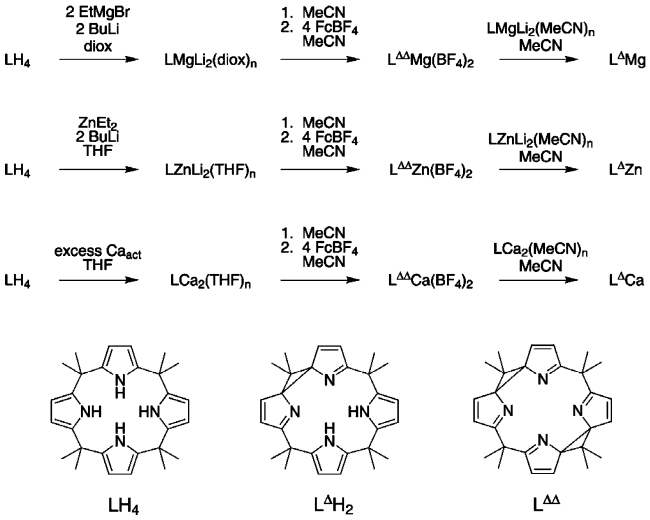

The three redox states of magnesium and calcium porphyrinogen, $[LM]^{2-}/[L^{\Delta}M]/[L^{\Delta\Delta}M]^{2+}$ (M = Mg, Ca), were prepared according to Scheme 1. The synthesis of the reduced members, $[LM]^{2-}$, required slight modifications to the

* To whom correspondence should be addressed. E-mail: nocera@mit.edu.

(1) Allen, G. C.; Hush, N. S. *Prog. Inorg. Chem.* **1967**, *8*, 357−389.
(2) Hush, N. S. *Prog. Inorg. Chem.* **1967**, *8*, 391−444.
(3) Robin, M. B.; Day, P. *Adv. Inorg. Chem. Radiochem.* **1967**, *10*, 247−422.
(4) Tom, G. M.; Creutz, C.; Taube, H. *J. Am. Chem. Soc.* **1974**, *96*, 7827−7828.
(5) Klotz, I. M.; Czerlinski, G. H.; Fiess, H. A. *J. Am. Chem. Soc.* **1958**, *80*, 2920−2923.
(6) Day, P.; Smith, D. W. *J. Chem. Soc. A* **1967**, *7*, 1045−1046.
(7) Kaim, W.; Klein, A.; Glockle, M. *Acc. Chem. Res.* **2000**, *33*, 755−763.
(8) Londergan, C. H.; Kubiak, C. P. *Chem. Eur. J.* **2003**, *9*, 5962−5969.
(9) Demadis, K. D.; Hartshorn, C. M.; Meyer, T. J. *Chem. Rev.* **2001**, *101*, 2655−2685.
(10) Creutz, C. *Prog. Inorg. Chem.* **1983**, *30*, 1−73.
(11) Bachmann, J.; Nocera, D. G. *J. Am. Chem. Soc.* **2004**, *126*, 2829−2837.
(12) Bachmann, J.; Nocera, D. G. *J. Am. Chem. Soc.* **2005**, *127*, 4730−4743.

10.1021/ic0511017 CCC: $30.25
Published on Web 09/01/2005

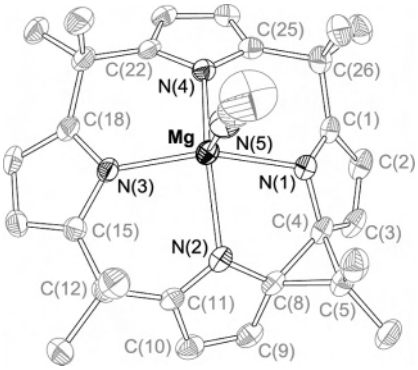

Figure 1. Thermal ellipsoid plot (50% probability level) for the solid-state structure of $[L^{\Delta}Mg(NCMe)]\cdot CH_2Cl_2$.[14]

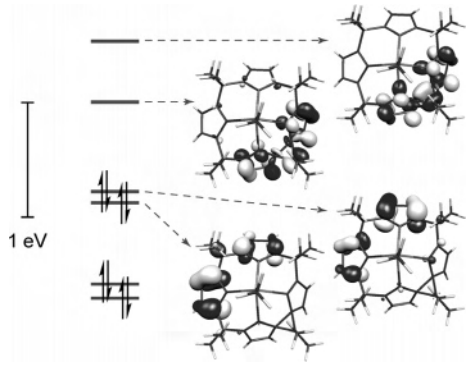

Figure 2. Computed frontier Kohn−Sham orbital diagram of the HOMOs and LUMOs of $[L^{\Delta}Mg(NCMe)]$.

procedure previously used for the preparation of $[LZn]^{2-}$. The lithium salt of $[LMg]^{2-}$ was obtained by reaction of diethylmagnesium, generated in situ from ethylmagnesium chloride in 1,4-dioxane, and butyllithium with LH_4. In the case of calcium, the preference of the constrained doubly oxidized macrocycle, $L^{\Delta\Delta}$, for small cations forced us to avoid Li^+ altogether and prepare $[LCa_2]$ from LH_4 and activated calcium.[13] $[L^{\Delta\Delta}M]^{2+}$ and $[L^{\Delta}M]$ were then obtained directly from $[LM]^{2-}$, as described in Scheme 1.

The crystal structure of $[L^{\Delta}Mg(NCMe)]\cdot CH_2Cl_2$, displayed in Figure 1, shows that the partly oxidized macrocycle is composed of a methylene-bridged dipyrrole dianion that is doubly strapped to a two-electron-oxidized dipyrrole. The latter is bridged by an almost equilateral cyclopropane ring (Δ): C(4)−C(5)−C(8) = 61.4(3)°, d(C(4)−C(8)) = 1.562(7) Å. The oxidized pyrroles show a clear bond alternation (d_{avg}(N(1)−C(1),N(2)−C(11)) = 1.30 Å, d_{avg}(N(1)−C(4),N(2)−C(8)) = 1.44 Å), whereas the neighboring pyrroles of the dianion are essentially symmetrical (d_{avg}(N(3)−C(15),N(4)−C(25)) = 1.38 Å, d_{avg}(N(3)−C(18),N(4)−C(22)) = 1.38 Å). This solid-state structure displays the same space group and same cocrystallized solvent molecule as that observed for $[L^{\Delta}Zn(NCMe)]\cdot CH_2Cl_2$.[11] More striking, the geometric parameters of the organic periphery in $[L^{\Delta}Mg(NCMe)]$ and $[L^{\Delta}Zn(NCMe)]$ are identical within uncertainty. The only significant structural difference between the two is in the position of the metal dication within the macrocycle. Whereas both Mg^{2+} and Zn^{2+} lie closer to the dipyrrole dianion than to the oxidized dipyrrole, Zn^{2+} is displaced further from the central core: d_{avg}(M−N(3,4)) = 2.08 Å (M = Mg) vs 2.02 Å (M = Zn). The positional difference between Zn and Mg is inversely related to the ionic radius ($r_{Mg^{2+}}$ = 0.86 Å and $r_{Zn^{2+}}$ = 0.88 Å)[15] and appears to be related to the pocket size of the two dipyrrole halves. The coordinating nitrogens of the dipyrrole dianion are considerably farther apart than those of the oxidized dipyrrole, which are strapped by the base of the cyclopropane: d(N(3)···N(4)) = 3.02 Å vs d(N(1)···N(2)) = 2.69 Å. The confluence of the larger pocket size on the reduced side of the macrocycle and the smaller pocket size on the oxidized side of the macrocycle appears to effectively "push" the larger cation away from N(1)/N(2) of the oxidized dipyrrole and into N(3)/N(4) of the dipyrrole dianion. This trend is consistent with data from the related d^7−d^9 octaethylporphyrinogen series $[^{Et}L^{\Delta}M]$, M = Co, Ni, Cu, reported by Floriani,[16,17] in which the metal ion lies in a roughly square-planar geometry: Ni^{2+} is the most centrally situated of the three ions, followed by Co^{2+} and Cu^{2+}. We note, however, that the significant electrostatic contribution to metal-ligand bonding in $[L^{\Delta}Mg(NCMe)]$ and $[L^{\Delta}Zn(NCMe)]$ translates into much larger differences in M−N bond lengths. In the case of the presently reported Mg/Zn/Ca series, the limited thermal stability of $[L^{\Delta}Ca]$ in solution hindered the growth of large single crystals, and accordingly a structural benchmark for the largest ionic member of the series could not be obtained.

Electronic consequences of the structural differences between the two sides of the porphyrinogen are evident in DFT calculations, the results of which are displayed in Figure 2. The energy level diagram is clearly demarcated about orbitals[18] with parentages derived from the oxidized and reduced sides of the ligand. The HOMOs are localized on the reduced dipyrroles, whereas the LUMOs are localized on the oxidized dipyrroles of $[L^{\Delta}]^{2-}$. The Kohn−Sham HOMO−LUMO gap is computed to be 0.82 eV for M = Zn and 0.72 eV for M = Mg. The smaller energy gap obtained for M = Mg relative to M = Zn arises from both a destabilization of the HOMO (+0.05 eV) and a stabilization of the LUMO (−0.05 eV). This result is consistent with simple electrostatic consideration of the position of the dication between the dipyrrole halves of the molecule. The MOs localized on the dipyrrole dianion will be stabilized as

(13) Bonomo, L.; Dandin, O.; Solari, E.; Floriani, C.; Scopelliti, R. *Angew. Chem., Int. Ed.* **1999**, *38*, 913−915.

(14) Summary of crystallographic data for $[L^{\Delta}Mg(NCMe)]\cdot CH_2Cl_2$: empirical formula, $C_{31}H_{37}N_5MgCl_2$; T = 193(2) K; λ = 0.710 73 Å; crystal system and space group, triclinic and $P\bar{1}$; unit cell dimensions, a = 10.4274(7) Å, b = 10.6231(7) Å, c = 14.3549(10) Å, α = 81.9710(10)°, β = 85.0730(10)°, γ = 73.5010(10)°, V = 1507.90(18) Å^3 (Z = 2); abs coeff, 0.265 mm^{-1}; 7845 reflections (4327 independent, R_{int} = 0.0504), F(000) = 608; 2.01° < θ < 23.29°, 99.7% completeness to θ = 23.29°; index ranges, −11 = h = 10, −11 = k = 11, −15 = l = 15; 4327 data, 0 restraints, 362 param; GOF(F^2) = 1.028; R1($I > 2\sigma(I)$) = 0.0928, wR2($I > 2\sigma(I)$) = 0.2700, R1(all data) = 0.1104, wR2(all data) = 0.2899; largest diffraction peak and hole, 0.690 and −1.222 e·Å^{-3}.

(15) Shannon, R. D. *Acta Crystallogr.* **1976**, *A32*, 751−767.
(16) De Angelis, S.; Solari, E.; Floriani, C.; Chiesi-Villa, A.; Rizzoli, C. *J. Am. Chem. Soc.* **1994**, *116*, 5691−5701.
(17) De Angelis, S.; Solari, E.; Floriani, C.; Chiesi-Villa, A.; Rizzoli, C. *J. Am. Chem. Soc.* **1994**, *116*, 5702−5713.
(18) Kohn, W.; Becke, A. D.; Parr, R. G. *J. Phys. Chem.* **1996**, *100*, 12974−12980.

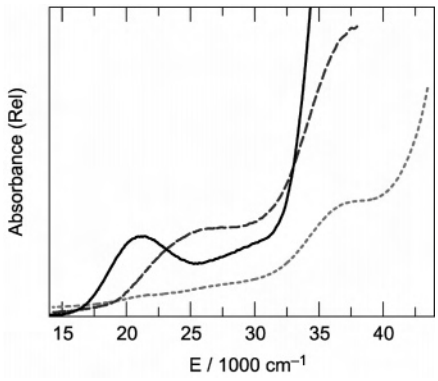

Figure 3. UV−visible absorption spectra of [L$^{\Delta}$Mg] (—), [L$^{\Delta}$Zn] (− −), and [L$^{\Delta}$Ca] (- - -) in CH_2Cl_2.

the dication moves toward it. At the same time, those on the oxidized dipyrrole will be destabilized as the electropositive metal center is moved further away. The trend in the HOMO−LUMO gap is paralleled by the IVCT absorption band, which blue shifts along the series [L$^{\Delta}$Mg] ($E_{IVCT,max}$ = 21 000 cm^{-1}) < [L$^{\Delta}$Zn] ($E_{IVCT,max}$ = 24 800 cm^{-1}) < [L$^{\Delta}$Ca] ($E_{IVCT,max}$ = 37 000 cm^{-1}) (Figure 3). The results suggest that the largest dication, Ca^{2+}, is most effective at stabilizing the HOMO and destabilizing the LUMO.

The position of the dication between the dipyrroles is also manifested in the computed dipole moment of the molecules. The ground state of the [L$^{\Delta}$]$^{2-}$ macrocycle is significantly polarized owing to the two-electron difference between dipyrrole subunits. Movement of the dication closer to the dipyrrole dianion should serve to diminish the dipole. This is observed in DFT calculations of [L$^{\Delta}$M(NCMe)] in its ground-state geometry: μ = 11.9 D for M = Zn and μ = 12.4 D for M = Mg. The ground-state dipole should be significantly diminished by the electron redistribution accompanying IVCT excitation. Accordingly, polar solvents should stabilize the ground state of [L$^{\Delta}$M] relative to its lowest-energy IVCT excited state. Experimentally, the energy of the IVCT transition should consequently blue shift as the polarity of the solvent increases; on the basis of the computed μ, this blue shift should be greater for M = Mg. Indeed, this is the case. Absorption spectra of [L$^{\Delta}$M] in CH_2Cl_2 and toluene show that $\Delta E_{IVCT,max}$ = 1600 cm^{-1} for [L$^{\Delta}$Mg] as compared to $\Delta E_{IVCT,max}$ = 900 cm^{-1} for [L$^{\Delta}$Zn].

In summary, IVCT is sensitive to the intervening bridge of the redox termini. Heretofore, the bridge has been typically a ligand that connects one-electron disparate metal ions. Changes in the bridge cause variations in electronic coupling as well as distance, and the IVCT energy is consequently related to the bridge in a complicated way.[9,19−21] This is not the case for the system described here. The IVCT depends on a single structural parameter: the position of the central metal between redox termini, which are also unique inasmuch as they are ligand-based and derive their mixed valency from a two-electron inequivalency.

Acknowledgment. We thank Dr. Lucia Bonomo and Dr. Geoffroy Guillemot for the information they provided with regard to the preparation of activated calcium. This work was supported by the National Science Foundation (Grant CHE-0450058). J.B. gratefully acknowledges predoctoral funding from the MIT Presidential Fellowship program and the Shell Oil Company.

Supporting Information Available: Experimental and computational procedures; DFT frontier orbital energies and Mulliken charges for [L$^{\Delta}$Mg(NCCH$_3$)]; tables of X-ray crystallographic data for [L$^{\Delta}$Mg(NCCH$_3$)]·CH_2Cl_2; X-ray crystallographic file in CIF format. This material is available free of charge on the Internet at http://pubs.acs.org.

IC0511017

(19) Lambert, C.; Risko, C.; Coropceanu, V.; Schelter, J.; Amthor, S.; Gruhn, N. E.; Durivage, J. C.; Bredas, J.-L. *J. Am. Chem. Soc.* **2005**, *127*, 8508−8516.
(20) Brunschwig, B. S.; Creutz, C.; Sutin, N. *Chem. Soc. Rev.* **2002**, *31*, 168−184.
(21) Barbara, P. F.; Meyer, T. J.; Ratner, M. A. *J. Phys. Chem.* **1996**, *100*, 13148−13168.